Chapter 5

Wide-Field Integration Methods for Visuomotor Control

J. Sean Humbert, Joseph K. Conroy, Craig W. Neely, and Geoffrey Barrows

Abstract In this chapter wide-field integration (WFI) methods, inspired by the spatial decompositions of wide-field patterns of optic flow in the insect visuomotor system, are reviewed as an efficient means to extract visual cues for guidance and navigation. A control-theoretic framework is described that is used to quantitatively link weighting functions to behaviorally relevant interpretations such as relative orientation, position, and speed in a corridor environment. The methodology is demonstrated on a micro-helicopter using analog VLSI sensors in a bent corridor.

5.1 Introduction

In recent years robotics research has seen a trend toward miniaturization, supported by breakthroughs in microfabrication, actuation, and locomotion [24], as described in Chap. 16. Engineers are on the verge of being able to design and manufacture a variety of microsystems; however, the challenge is to endow these creations with a sense of autonomy that will enable them to successfully interact with their environments. Scaling down traditional paradigms will not be sufficient due to the stringent size, weight, and power requirements of these vehicles (Chap. 21). Novel sensors and sensory processing architectures will need to be developed if these efforts are to be ultimately successful.

J.S. Humbert (✉)
Autonomous Vehicle Laboratory, University of Maryland, College Park, MD USA
e-mail: humbert@umd.edu

Recently there has been considerable interest [1] (see Chaps. 2, 3, and 6) in utilizing optic flow for navigation as an alternative to the more traditional methods of computer vision [12] and machine vision [4]. The general approach has been to extract qualitative visual cues from optic flow and use these directly in a feedback loop. One example is the detection of expansion, which can be used as an indication of an approaching obstacle. In [22] it was shown that simple models of integrated expansion on the left versus the right eyes of fruit flies accounted well for saccadic behavior of freely flying animals in an arena. This technique was successfully implemented by Zufferey et al. (Chap. 6) where reflexive obstacle avoidance was demonstrated on lightweight, propeller-driven airplane.

Navigation methods based on optic flow are mostly inspired by the insightful work of Srinivasan et al. (Chap. 2) who postulated a well-known heuristic, the centering response, observed in honeybees as they traversed a corridor. This heuristic states that in order to negotiate a narrow gap, an insect must balance the image velocity on the left and right retinas, respectively. Local navigation utilizing this centering technique has been described in recent approaches [19, 15], as well as by Franceschini et al. (see Chap. 3). An excellent review and summary of earlier work is given in [8].

In this chapter the method of wide-field integration is reviewed, an analogue to tangential cell processing inspired by the spatial decompositions of optic flow in the insect visuomotor system. The concept is based on extracting information for navigation by spatially decomposing wide-field patterns of optic flow with sets of weighting functions. Outputs are interpreted as encoding information about relative speed and proximity with respect to obstacles in the surrounding

D. Floreano et al. (eds.), *Flying Insects and Robots*,
DOI 10.1007/978-3-540-89393-6_5,

environment, which are used directly for feedback. The methodology described herein is demonstrated on a ground vehicle and a micro-helicopter navigating corridor environments of varying spatial structure. In both examples, weighted sums of the instantaneous optic flow field about the yaw axis are used to extract relative heading and lateral position (and, in addition, relative speed for the ground vehicle). The resulting closed-loop responses replicate the navigational heuristics described by Srinivasan in Chap. 2.

5.2 The Insect Visuomotor System

The insect retina can be thought of as a map of the patterns of luminance of the environment. As an insect moves, these patterns become time dependent and are a function of the insect's relative motion and proximity to objects through motion parallax. The rate and direction of these local image shifts, taken over the entire visual space, form what is known as the optic flow field (see Chap. 6, Sect. 6.3). Local estimates of optic flow are thought to be computed by correlation-type motion detectors in the early portion of the visual pathway. Subsequently, these outputs are pooled by approximately 60 tangential neurons in the third visual neuropile of each hemisphere (see Chap. 4, Sect. 4.3), a region referred to as the *lobula plate* (Fig. 5.1A). Extraction of wide-field visual information occurs at the level of these tangential cells, which spatially decompose complicated motion patterns over large swaths of the visual field into a set of feedback signals used for stabilization and navigation [5, 2]. Descending cells, which receive dendritic input from tangential cells, connect to the neurons in the flight motor to execute changes in wing kinematics.

Tangential cells respond selectively to stimuli by either graded shifts in membrane potential or changes in spiking frequency, depending on class [9]. Shifts are depolarizing (or spiking frequency increases) if the motion pattern is in the preferred direction and hyperpolarizing (or spiking frequency decreases) in the null direction [10, 11]. In addition to direction selectivity, tangential cells also exhibit spatial selectivity within their receptive fields [10, 11, 18, 17], as shown in Fig 5.1B.

Due to their motion sensitivity patterns, which are similar to the equivalent projected velocity fields for certain cases of rotary self-motion, it has been postulated that tangential cells function as direct estimators of rotational velocity [17]. However, recent work has shown that translational motion cues, which are the source of proximity information, are also present in the outputs of cells that were previously thought to be used only for compensation of rotary motion (Chap. 4, Sect. 4.2). This suggests that cell patterns might be structured to extract a combination of relative

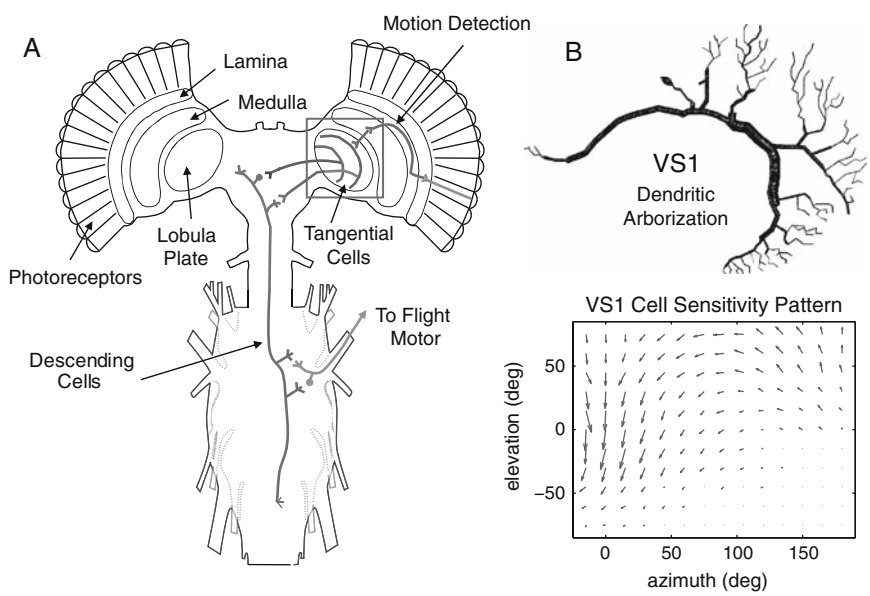

Fig. 5.1 (**A**) Visuomotor system structure, (**B**) VS1 tangential cell and associated wide-field sensitivity pattern. The data were extracted and replotted from [17]

speed and proximity cues, rather than direct estimates of the velocity state. Hence, significant progress has been made in understanding structure, arrangement, and synaptic connectivity [5]; however, the exact functional role that each of these neurons hold in the flight control and navigation system of the fly remains a challenging and open question.

5.3 Wide-Field Integration of Optic Flow

The goal of this research is to investigate how the spatial decompositions of optic flow by tangential cells, described here as *wide-field integration*, might be used in closed-loop feedback to explain the visual-based behaviors exhibited by insects. The approach is based on a novel premise: tangential cells are not used to directly estimate self-motion quantities of a flying organism as in traditional implementations [7, 6]. Rather, it is assumed their purpose is to detect departures from desired patterns of optic flow, generating signals that encode information with respect to the surrounding environment. The resulting set of signals can be used in a feedback loop to maintain a safe distance from obstacles in the immediate flight path.

The intuition behind this approach is shown in Fig 5.2. Forward motion of a vehicle constrained to move in 3 DOF (forward and lateral translation along with yaw rotation) in the horizontal plane generates an optic flow pattern with a focus of expansion in the front field of view, a focus of contraction in the rear, with the largest motion on the sides. If plotted as a function of the angle δ around the retina, this is approximately a sine wave (Fig. 5.2A). Perturbations from this equilibrium state of a constant forward velocity u_0 along the centerline of the tunnel introduce either an *asymmetry* in this signal for lateral displacements δy (Fig. 5.2B) or a *phase shift* for rotary displacements $\delta\psi$ (Fig. 5.2C). If the forward speed is increased by δu, the *amplitude* of this signal increases (Fig. 5.2D), and if the vehicle is rotating at angular velocity $\dot{\psi}$ about the yaw axis a DC shift in the signal of equal magnitude occurs. Therefore, the amplitude, phase, and asymmetry of the pattern of optic flow around the yaw axis encode important information that could be used for navigation and speed regulation.

The structure of the visuomotor pathway of insects (Fig. 5.1A) gives us a hint as to how extracting this type information from patterns of optic flow might be achieved simply and quickly. Tangential cells, which parse the complicated patterns of optic flow generated during locomotion, exhibit either a shift in membrane potential or an increase in spike frequency when they are presented with a wide-field pattern they are tuned to. Essentially, each cell makes a *comparison* between its preferred pattern sensitivity and the pattern of the stimulus. Mathematically, this process can be represented as an *inner product* $\langle u,v\rangle$, analogous to the dot

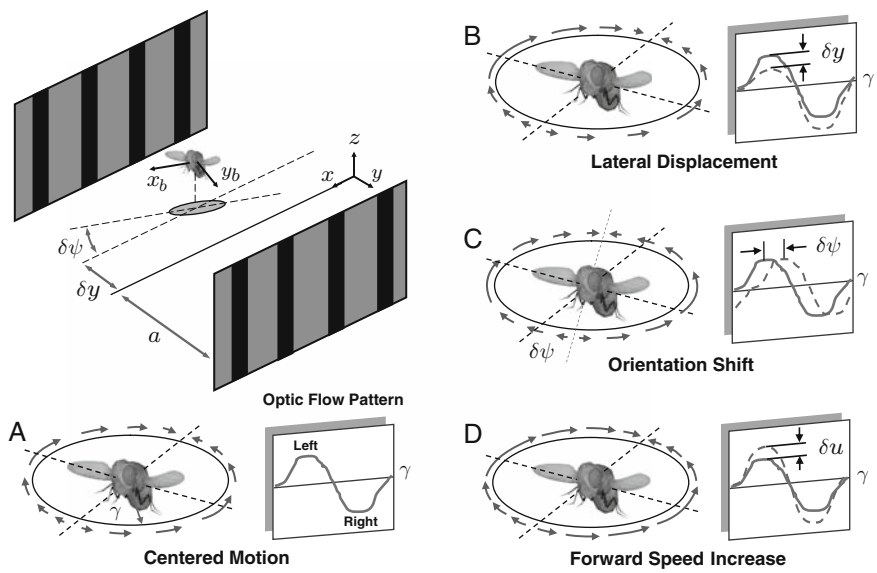

Fig. 5.2 Perturbations of azimuthal optic flow and their correlations to the relative state of the vehicle. Amplitude, phase, and asymmetry of the azimuthal optic flow pattern encode relative proximity and speed with respect to obstacles in the environment

product between vectors, which tells us how similar two objects u and v are.

In the case of Fig. 5.2, the patterns are assumed to reside in $L_2[0,2\pi]$, the space of 2π-periodic and square-integrable functions, where the inner product is given by

$$z_i(x) \;=\; \langle \dot{Q}, F_i \rangle \;=\; \int_0^{2\pi} \dot{Q}(\gamma, x) \cdot F_i(\gamma)\, d\gamma. \quad (5.1)$$

Here $\dot{Q}(\gamma, x)$ is the measured optic flow about the yaw axis, $F_i(\delta)$ is any square-integrable weighting function such that (5.1) exists, and $z_i(x)$ is the resulting output which is a function of the relative state x (proximity and velocity) of the insect with respect to the environment. This expression, which could represent either a shift in membrane potential or a change in spiking frequency, gives a number that is maximum if the patterns line up, negative if the pattern has the same structure but is in the opposite direction, and zero if the patterns are completely independent (orthogonal) of one another. The resulting set of outputs represents a decomposition of the motion field into simpler pieces that encode perturbations from the desired pattern.

Navigation behavior can be achieved by implementing a feedback loop which attempts to maintain a sine wave pattern of optic flow (Fig. 5.2A) on the circular imaging surface. Departures from the desired relative state create spatial perturbations that can be extracted with the above *tangential cell analogue* (5.1). For example, an estimate of the phase shift is given by integrating $\dot{Q}$ against an $F(\gamma) = \cos\gamma$ weighting function, relative speed results from integrating $\dot{Q}$ against an $F(\gamma) = \sin\gamma$ weighting function, and asymmetry can be extracted with an $F(\gamma) = \cos 2\gamma$ weighting function. These correspond to the first cosine a_1, first sine b_1, and second cosine a_2 Fourier harmonics of the optic flow signal. These low-order spatial harmonics yield the orientation, speed, and lateral position relative to the corridor and can be used as feedback commands to maneuver the vehicle accordingly to maintain the desired sine wave pattern of optic flow.

Rotational motion $\dot{\psi}$ about the yaw axis also introduces an asymmetry between the left and right values of the optic flow signal; however, since the result is a pure DC shift, the $F(\gamma) = \cos 2\gamma$ weighting extracts only the portion of the asymmetry due to a lateral displacement δy. To extract the rotational motion $\dot{\psi}$ directly, a function which is a combination of a DC shift and a $\cos 2\gamma$ weighting would be required as a lateral displacement δy also introduces a change in the DC value of the signal.

Something similar occurs when attempting to extract the relative heading. A pure orientation offset $\delta\psi$ creates a phase shift in all the harmonics of the optic flow signal; however, a lateral velocity δv will introduce a shift in only the low-frequency harmonics. This is not an issue for platforms which have sideslip constraints such as a ground vehicle [14]. For other platforms such as hovercraft or helicopters, a coupling between the orientation ψ and lateral position y degrees of freedom is introduced which has a detrimental effect on the achievable closed-loop bandwidth in the lateral degree of freedom [15]. The extension of the proposed wide-field integration methodology to 3D environments and 6-DOF vehicles has shown that this issue can be resolved by utilizing optic flow about either the pitch or roll axis, which can be used to unambiguously decouple the two distinct motions [16].

The primary advantage of this framework is that it can be used to quantitatively link weighting functions to interpretations such as relative orientation, position, and speed, as shown above. For standard obstacles (one wall, two walls, cylinders, etc.) one can express $\dot{Q}$ in closed form, analytically compute (5.1), and subsequently linearize about the state corresponding to desired equilibrium pattern of optic flow. This results in an output equation $y = Cx$, which is a linear function of the relative state. Analysis tools from control theory, such as output LQR [21], can then be applied to derive gains for desired stability and performance.

Results from an experimental implementation on a wheeled robot [13] are shown in Fig. 5.3. Optic flow is computed using an *OpenCV* implementation of the Lucas–Kanade algorithm around a 360° ring from imagery generated by a vertically mounted camera which points upward at a parabolic mirror. Spatial harmonics (integral weightings) of optic flow, encoding perturbations from the equilibrium pattern, are used as control inputs to maneuver the vehicle. Regulation of the sine wave pattern on the mirror is achieved by using these signals as feedback to force or torque accordingly. Therefore, this simple visuomotor control architecture (wide-field integration) gives rise to the centering and clutter navigational heuristics observed in insect behavior [20].

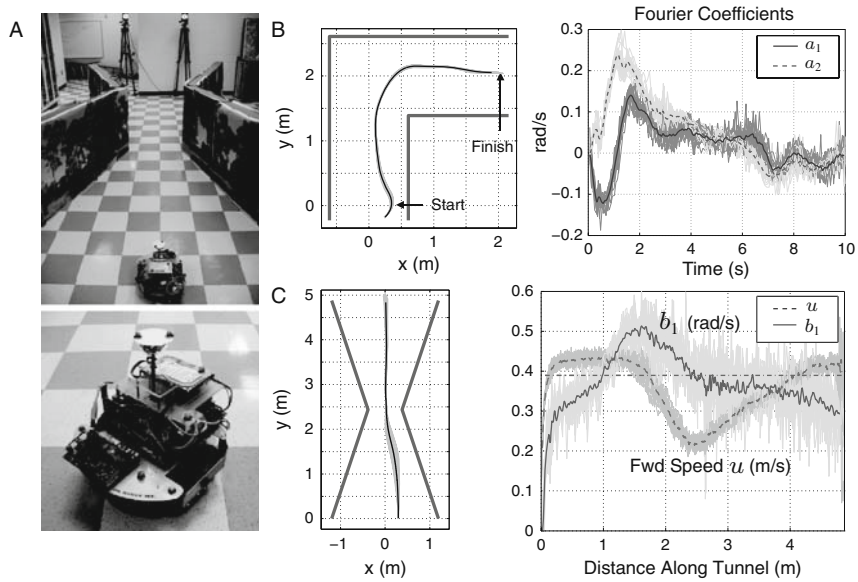

Fig. 5.3 (**A**) Autonomous corridor navigation of a ground vehicle using wide-field integration techniques. (**B**) Navigation of a 90° bend. The mean values of the position in the corridor along with all 20 individual trials are plotted for a combined lateral and rotational offset, along with the corresponding Fourier harmonics a_1 and a_2 of the optic flow signal. (**C**) Converging–diverging corridor navigation. The first sine harmonic b_1 of the optic flow is held constant over 20 runs by modulating the forward speed, resulting in a speed decrease as the vehicle navigates the narrow gap

5.4 Application to a Micro-helicopter

The preceding experimental implementation of optic flow-based navigation on the ground vehicle has been extended to the case of an electric micro-helicopter (Fig. 5.4A). The goal in this demonstration is to provide autonomous navigation of a bent corridor environment using estimates of relative heading and lateral position derived from weighted sums of the instantaneous optic flow field about the yaw axis. Pitch, roll, and forward speed control of the helicopter is accomplished with an external marker-based visual tracking system while the heading and lateral control loops are closed using optic flow-derived estimates. No altitude control is required as the helicopter is sufficiently stable for a constant thrust in ground effect. Optic flow is measured in a tangential ring arranged around the azimuth of the helicopter (Fig. 5.4B). Due to a lack of available payload for the camera and parabolic mirror configuration, VLSI sensors are used for optic flow estimation. The increased noise inherent in the VLSI implementation of the optic flow algorithms (see Chap. 8) along with the increased vibrations present on the helicopter reduces the quality of the optic flow estimates. It is demonstrated, however, that the wide-field integration methodology is sufficient to affect navigation capabilities.

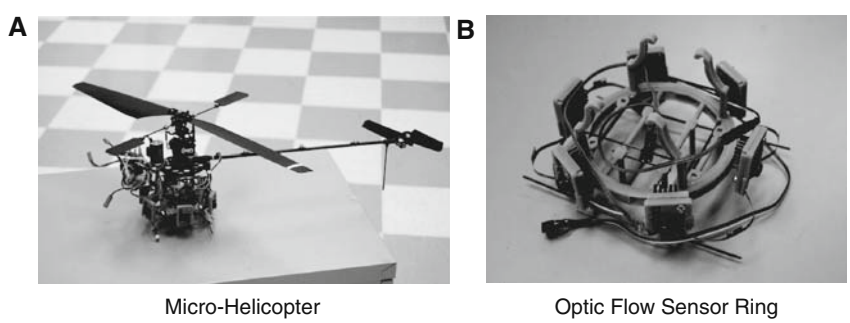

Fig. 5.4 (**A**) E-Sky Honeybee micro-helicopter, and (**B**) optic flow sensor ring with six ARZ-Lite sensors from Centeye, Inc

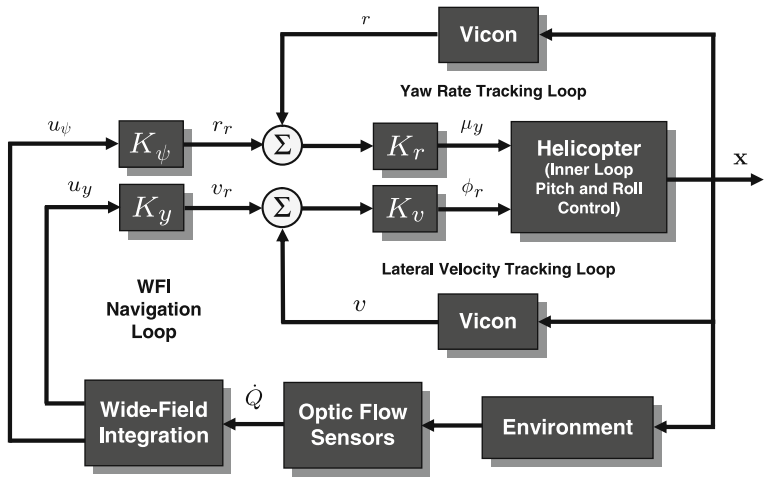

Fig. 5.5 Closed-loop block diagram for WFI-based navigation. Inner loop pitch and roll control are accomplished using Vicon measurements while optic flow-derived outputs are used to close the outer navigation loop

For a helicopter, the high-order dynamics and a large degree of coupling require additional consideration, thus making implementation more complex than that of the ground vehicle. Additionally, the motion is unconstrained such that sideslip, forward speed, and rotation can all be varied independently. A state-space model of the helicopter dynamics, linearized about the hover condition, has been identified in prior work [3]. This identified model confirms that the lateral and longitudinal dynamics are highly coupled and of high order. Additionally, the heading degree of freedom is highly sensitive to the yaw input and disturbances due to the low rotational damping and inertia. This degree of freedom is immediately modified via onboard integrated yaw rate feedback to add additional damping. While the helicopter is clearly not a planar constrained vehicle in general, given a fixed altitude and non-aggressive maneuvers, a planar analysis and implementation can be assumed.

A Vicon^{TM} visual tracking system provides an offboard feedback capability that reduces the effective dynamics of the vehicle. Direct measurements of the vehicle state $\mathbf{x} = (x,y,\psi,u,v,r)$ are available at 350 Hz at 10 ms latency and provide ground truth data for the experiment. Attitude feedback for the roll and pitch degrees of freedom greatly reduces the cross-coupling effects inherent in the dynamics, thus allowing the lateral and longitudinal degrees of freedom to be considered separately. The resulting set of reduced order dynamics is given by

$$\begin{aligned} \dot{v} &= Y_v v + g\phi_r \\ \dot{u} &= X_u u - g\theta_r, \end{aligned} \tag{5.2}$$

where Y_v and X_u are aerodynamic damping derivatives [23], g is gravity, and ϕ_r and θ_r are the commanded orientation values for roll and pitch, respectively. For low frequencies these can be considered to be the same as the actual roll and pitch values, ϕ and θ. The corresponding transfer function form, given only for the lateral degree of freedom, is

$$\frac{v}{\phi_r} = \frac{g}{s + Y_v}. \tag{5.3}$$

The effective lateral and longitudinal transfer functions can be further modified via a simple proportional velocity tracking feedback using a Vicon estimate for the lateral velocity v (Fig. 5.5). Given a control gain K_v and a commanded velocity v_r, the resulting transfer function for the lateral degree of freedom is

$$\frac{v}{v_r} = \frac{K_v g}{s + (Y_v + K_v g)}. \tag{5.4}$$

A transfer function of identical form is valid for the longitudinal degree of freedom. The velocity tracking loop further reduces the effect of the cross-coupling in the vehicle dynamics and adds effective damping. In the current experiment (Fig. 5.6) the forward commanded velocity u_r is fixed to a constant value $u_0 = 0.6$ m/s, whereas the desired lateral velocity reference v_r can be used as a control input to laterally maneuver the helicopter.

Heading control is also augmented using the visual tracking system to supply rate tracking capability. The open-loop heading dynamics are given as

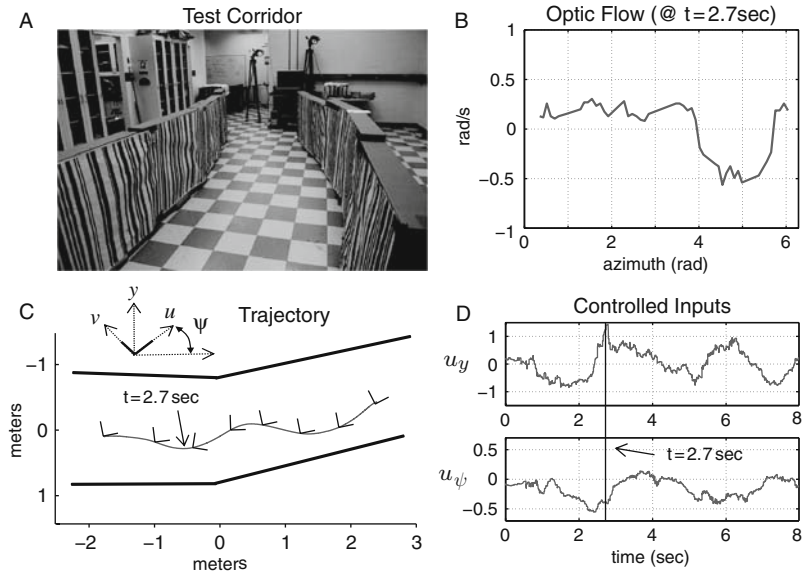

Fig. 5.6 (**A**) Bent corridor test environment, (**B**) azimuthal optic flow pattern $\dot{Q}$ measured at time $t = 2.7$, (**C**) helicopter trajectory through the corridor along with the relative heading given by the angle of the L-shaped markers with respect to the vertical, and (**D**) time history of the controlled inputs u_y and u_ψ.

$$\dot{r} = N_r r + N_{\mu_y}\mu_y, \tag{5.5}$$

where r is the yaw rate, N_r is the yaw damping, $N_{\mu y}$ is the control sensitivity, and μ_y is the tail motor input. The term N_r is naturally aerodynamic in origin; however, we include in this term the effects of the onboard yaw rate damping as well. Simple proportional feedback is again used to provide yaw rate tracking capability (Fig. 5.5), resulting in the following transfer function, from desired reference rate, r_r, to the actual rate, r is:

$$\frac{r}{r_r} = \frac{K_r N_{\mu_y}}{s + (N_r + K_r N_{\mu_y})}. \tag{5.6}$$

The desired yaw velocity reference r_r can be used as a control input to modulate the heading of the helicopter.

We express the tangential component of the optic flow on a circular-shaped sensor that is constrained to 3-DOF motion in the horizontal plane for a general configuration of obstacles as follows:

$$\dot{Q}(\gamma,\mathbf{x}) = -r + \mu(\gamma,\mathbf{x})\,(u\sin\gamma - v\cos\gamma). \tag{5.7}$$

This expression is a 2π-periodic function in the viewing angle δ and the state of the vehicle $\mathbf{x} = (x,y,\psi,u,v,r)$. The function $\mu(\gamma,\mathbf{x}) = 1/d(\gamma,\mathbf{x})$ is defined as the nearness, where $d(\gamma,\mathbf{x})$ is a continuous representation of distance to the nearest point in the visual field from the current pose of the vehicle within the environment.

For the case of a straight corridor, the nearness function $\mu(\gamma,\mathbf{x})$ is independent of the axial position and can be expressed in closed form as a function of the lateral position y, the relative body frame orientation ψ, and the tunnel half-width a:

$$\mu(\gamma,\mathbf{x}) = \begin{cases} \dfrac{\sin(\gamma+\psi)}{a-y} & 0 \le \gamma+\psi < \pi \\ -\dfrac{\sin(\gamma+\psi)}{a+y} & \pi \le \gamma+\psi < 2\pi \end{cases}. \tag{5.8}$$

The above lateral (5.4) and yaw (5.6) dynamics are provided in the body frame of reference. To facilitate the selection of the spatial weighting functions, we express these equations, along with (5.7), in terms of the pose of the vehicle, where x and y denote the longitudinal and lateral corridor positions, respectively, and the heading orientation is denoted as ψ. The equivalent reduced-order helicopter dynamics for the lateral and yaw degrees of freedom in the inertial frame of reference are

$$\begin{aligned} \ddot{y} &= -(Y_v + K_v g)\dot{y} + K_v g v_r \\ \ddot{\psi} &= -(N_r + K_r N_{\mu_y})\dot{\psi} + K_r N_{\mu_y} r_r. \end{aligned} \tag{5.9}$$

Outputs suitable for feedback are computed using (5.1), with weighting functions that extract the relative lateral position and orientation in the corridor. The estimate for the relative lateral position in the corridor $u_y = \langle \dot{Q}, F_y \rangle$ is obtained using the weighting function $F_y(\gamma) = \cos 2\gamma$. The orientation estimate $u_\psi = \langle \dot{Q}, F_\psi \rangle$ can be extracted using the weighting function $F_\psi(\gamma) = \sin 2\gamma$ for $0 \leq \gamma < \pi$ and $F_\psi(\gamma) = \sin 2\gamma$ for $\pi \leq \gamma < 2\pi$. The choice of $F_\psi(\gamma)$, while providing the same linearized signal content as $\cos \gamma$, maximally weights the optic flow field in regions where it has the best signal-to-noise ratio, hence is more robust for experimental implementation. The controlled inputs (Fig. 5.5) are then given by

$$\begin{aligned} v_r &= K_y \langle \dot{Q}, F_y \rangle \\ r_r &= K_\psi \langle \dot{Q}, F_\psi \rangle. \end{aligned} \tag{5.10}$$

The analytical result of these spatial inner products is nonlinear; however, each inner product can be linearized about the desired optic flow pattern, corresponding to motion at a fixed speed $u_r = u_0$ along the centerline of the corridor, to determine the linear output equation. When combined with (5.9), the resulting closed-loop linearized dynamics are

$$\begin{Bmatrix} \dot{y} \\ \ddot{y} \\ \dot{\psi} \\ \ddot{\psi} \end{Bmatrix} = \begin{bmatrix} 0 & 1 & 0 & 0 \\ -K_y \frac{u_0 K_v g}{2a^2} & -(Y_v + K_v g) & 0 & 0 \\ 0 & 0 & 0 & 1 \\ 0 & K_\psi \frac{K_r N_{\mu_y}}{2a} & -K_\psi \frac{u_0 K_r N_{\mu_y}}{a} & -(N_r + N_{\mu_y} K_r) \end{bmatrix} \begin{Bmatrix} y \\ \dot{y} \\ \psi \\ \dot{\psi} \end{Bmatrix}. \tag{5.11}$$

The feedback gains K_y and K_ψ, which determine the amount of lateral and rotational stiffness added to the dynamics, can be adjusted to position closed-loop eigenvalues for desired stability and performance.

A test utilizing a bent corridor (Fig. 5.6A) was conducted to demonstrate the wide-field integration-based feedback on a micro-helicopter. Six equally spaced VLSI hard-coded sensors from Centeye were used for optic flow estimation (Fig. 5.4B). Eight points were taken from the 45° field of view of each sensor, resulting in a set of 48 optic flow measurements. A representative trajectory and optic flow pattern are shown in Fig. 5.6B. The relative heading of the vehicle at various points on the trajectory is given by the angle of the L-shaped markers with respect to the vertical (Fig. 5.6C). This test demonstrates the potential for using the wide-field integration architecture to fuse relatively noisy optic flow estimates (measured on a vibrating platform) to provide feedback sufficient for navigation.

5.5 Summary

In this chapter we have reviewed wide-field integration (WFI) methods for visuomotor control, which are based on the spatial decompositions of wide-field patterns optic flow in the insect visuomotor system. By decomposing patterns of optic flow with weighting functions, one can extract signals that encode relative proximity and speed with respect to obstacles in the environment, which are used directly for visual navigation feedback. The methods discussed have been grounded in a theoretical framework and can be analyzed using traditional control system design tools. In addition, these methods have the advantages of computation speed and simplicity, hence are consistent with the stringent size, weight, and power requirements of MAVs.

Acknowledgments The support for this research was provided in part by the Army Research Office under grants DAAD19-03-D-0004 and Army-W911NF0410176, and the Air Force Research Laboratory under contract FA8651-07-C-0099. The authors would also like to thank Andrew M. Hyslop and Evan R. Ulrich for contributions to the work presented.

References

1. Barrows, G., Chahl, J., Srinivasan, M.: Biologically inspired visual sensing and flight control. The Aeronautical Journal **107**, 159–168 (2003)
2. Borst, A., Haag, J.: Neural networks in the cockpit of the fly. Journal of Comparative Physiology A **188**, 419–437 (2002)
3. Conroy, J., Pines, D.: System identification of a miniature electric helicopter using mems inertial, optic flow,

and sonar sensing. Proceedings of the American Helicopter Society. Virginia Beach, VA (2007)
4. Davies, E.R.: Machine Vision: Theory, Algorithms, Practicalities. Morgan Kaufmann, San Francisco, CA (2005)
5. Egelhaaf, M., Kern, R., Krapp, H., Kretzberg, J., Kurtz, R., Warzecha, A.: Neural encoding of behaviourally relevant visual-motion information in the fly. Trends in Neurosciences **25**, 96–102 (2002)
6. Franz, M., Chahl, J., Krapp, H.: Insect-inspired estimation of egomotion. Neural Computation **16**, 2245–2260 (2004)
7. Franz, M., Krapp, H.: Wide-field, motion-sensitive neurons and matched filters for optic flow fields. Biological Cybernetics **83**, 185–197 (2000)
8. Franz, M., Mallot, H.: Biomimetic robot navigation. Robotics and Autonomous Systems **30**, 133–153 (2000)
9. Hausen, K.: Motion sensitive interneurons in the optomotor system of the fly, part i. the horizontal cells: structure and signals. Biological Cybernetics **45**, 143–156 (1982)
10. Hausen, K.: Motion sensitive interneurons in the optomotor system of the fly, part ii. the horizontal cells: Receptive field organization and response characteristics. Biological Cybernetics **46**, 67–79 (1982)
11. Hengstenberg, R., Hausen, K., Hengstenberg, B.: The number and structure of giant vertical cells (vs) in the lobula plate of the blowfly *Calliphora erythrocephala*. Journal of Comparative Physiology. **149**, 163–177 (1982)
12. Horn, B.K.: Robot Vision. MIT Press and McGraw-Hill, Cambridge, MA (1986)
13. Humbert, J.S., Hyslop, A.M., Chinn, M.W.: Experimental validation of wide-field integration methods for autonomous navigation. Proceedings of the IEEE Conference on INtelligent Robots and Systems (IROS). San Diego, CA (2007)
14. Humbert, J.S., Murray, R.M., Dickinson, M.H.: A control-oriented analysis of bio-inspired visuomotor convergence (*submitted*). Proceedings of the 44th IEEE Conference on Decision and Control. Seville, Spain (2005)
15. Humbert, J.S., Murray, R.M., Dickinson, M.H.: Sensorimotor convergence in visual navigation and flight control systems. Proceedings of the 16th IFAC World Congress. Praha, Czech Republic (2005)
16. Hyslop, A., Humbert, J.S.: Wide-field integration methods for autonomous navigation of 3d environments. Proceedings of the AIAA Conference on Guidance, Navigation, and Control. Honolulu, HI (2008)
17. Krapp, H., Hengstenberg, B., Hengstenberg, R.: Dendritic structure and receptive-field organization of optic flow processing interneurons in the fly. Journal of Neurophysiology **79**, 1902–1917 (1998)
18. Krapp, H., Hengstenberg, R.: Estimation of self-motion by optic flow processing in single visual interneurons. Letters to Nature **384**, 463–466 (1996)
19. Santos-Victor, J., Sandini, G.: Embedded visual behaviors for navigation. Robotics and Autonomous Systems **19**, 299–313 (1997)
20. Srinivasan, M., Zhang, S., Lehrer, M., Collet, T.: Honeybee navigation *en route* to the goal: visual flight control and odometry. The Journal of Experimental Biology **199**, 237–244 (1996)
21. Stevens, B., Lewis, F.: Aircraft Control and Simulation. John Wiley & Sons, Inc., Hoboken, NJ (2003)
22. Tammero, L.F., Dickinson, M.H.: The influence of visual landscape on the free flight behavior of the fruit fly *Drosophila melanogaster*. The Journal of Experimental Biology **205**, 327–343 (2002)
23. Tichler, M., Remple, R.K.: Aircraft and Rotorcraft System Identification: Engineering Methods and Flight Test Examples. American Institute of Aeronautics and Astronautics, Inc., Reston, VA (2006)
24. Wood, R., Avadhanula, S., Sahai, R., Steltz, E., Fearing, R.: First takeoff of a biologially-inspired at-scale robotic insect. IEEE Transactions on robotics **24**(2), 341–347 (2008)